B978-1-78242-228-0.00013-2, 00013

c0065 Selective laser-induced graphene for patterning micro- and nanoscale photonic structures

13

Naili Yue[1], *Yong Zhang*[1,*]
[1]The University of North Carolina at Charlotte, Charlotte, NC, USA
*Corresponding author: Yong.Zhang@uncc.edu

s0010 13.1 Introduction

p0015 Since the initial experimental investigation of monolayer graphene by Novoselov and Geim (Novoselov et al., 2004) in 2004, graphene research has evolved from the exploration and development of synthesis techniques of large-size graphene (Novoselov et al., 2005; Zhang et al., 2005; Hass et al., 2008; Kim et al., 2009; Li et al., 2009) to the patterning of graphene nanostructures (GNSs) (Jiao et al., 2009; Kosynkin et al., 2009). Typically, GNSs are patterned on a large-size graphene film either by photolithography or electron beam lithography and plasma etching or obtained by unzipping a carbon nanotube (Jiao et al., 2009; Kosynkin et al., 2009). For both patterning methods, prepatterned graphene has to undergo wet lithography and dry etching processes, which incurs some defects or contaminations to the surface-sensitive graphene. Furthermore, the subsequent transfer process could cause additional perturbation to the morphology or introduce defects to the fragile two-dimensional (2D) graphene during transportation or handling. In contrast, laser-induced local graphene formation (LLG) is a quick and clean approach to synthesizing and patterning graphene. Various LLG techniques have been explored in recent years (Ohkawara et al., 2003; Perrone et al., 2009; Lee et al., 2010; Yue et al., 2012, 2013; Yannopoulos et al., 2012). Among these laser-based approaches for making graphene from SiC, most of these efforts focused on the surface conversion of bulk single-crystalline SiC into graphene. In contrast, our effort (Yue et al., 2012, 2013) focuses on the conversion from polycrystalline SiC thin film or prepatterned SiC micro- and nanostructures grown on Si wafer substrates using molecular beam epitaxy (MBE), and the development of techniques for generating patterned micro- and even nanoscale graphene structures. With the formation of the graphene structures directly on the Si wafer, the integration of graphene-based photonic and electronic devices with existing silicon-based microelectronics becomes more feasible. Furthermore, SiC micro- and nanostructures themselves are of great interest for a number of photonics-related applications.

Modeling, Characterization and Production of Nanomaterials. http://dx.doi.org/10.1016/B978-1-78242-228-0.00013-2

Comp. by: pdjeapradaban Stage: Proof Chapter No.: 13 Title Name: Tewary_and_Zhang
Date:5/12/14 Time:18:14:55 Page Number: 331

B978-1-78242-228-0.00013-2, 00013

s0015 13.2 Growth of 3C-SiC thin film on Si (111) using MBE

p0020 An ultrahigh-vacuum MBE system (with 10^{-10} Torr base pressure) was used to grow SiC thin films on Si substrates. Fullerene (C_{60}) powders were used as carbon sources, and the Si source was directly from the Si (111) wafer substrate. C_{60} is found to decompose when incident on the Si substrate then to react with Si from the substrate to form SiC, under an appropriate combination of substrate temperature (T_S) and C_{60} temperature (T_C) (Yue et al., 2013). In our MBE growth, the typical temperature ranges were T_S=700-800°C and T_C=500-600°C; T_S and T_C are silicon substrate and carbon source temperatures, respectively. The optimal combination was found to be T_S=800°C and T_C=550°C in terms of crystallinity and uniformity. During growth, the gas or vapor in the chamber was monitored with a mass spectrometer, and the film surface quality was inspected with reflection high-energy electron diffraction (RHEED). After 10 min of growth, the samples were held at the growth temperature for 5-10 min to homogenize the epitaxial film. Then, the film was allowed to cool down slowly (10°C/min) to room temperature. Figure 13.1 shows the XRD patterns of 3C-SiC grown on Si (111) and bare Si (111). It can be clearly seen that 3C-SiC (111), corresponding to 2θ=35.6°, was grown on Si (111). The surface morphology and cross-section images of a 3C-SiC (111) sample are shown in Figure 13.2, with polycrystalline grains of nearly uniform size and an average thickness of 188 nm.

p0025 Although the SiC grain size increases with increasing substrate temperature, the surface roughness also increases, which is undesirable for forming homogeneous graphene on top of the SiC thin film. However, the larger grain 3C-SiC requires higher

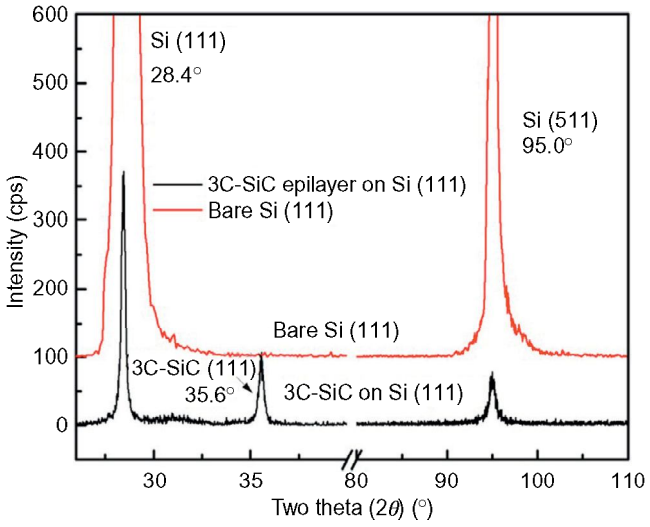

f0010 **Figure 13.1** XRD patterns of 3C-SiC grown on Si (111) and bare Si (111).

Comp. by: pdjeapradaban Stage: Proof Chapter No.: 13 Title Name: Tewary_and_Zhang
Date:5/12/14 Time:18:14:55 Page Number: 332

B978-1-78242-228-0.00013-2, 00013

 Au2

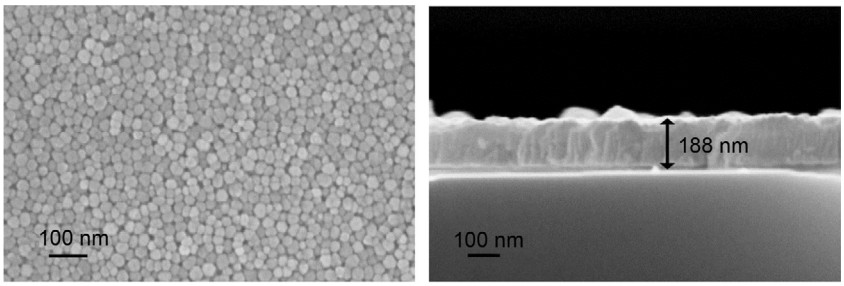

f0015 **Figure 13.2** SEM images of 3C-SiC (111) on Si (111). (a) Surface morphology, (b) cross-section.

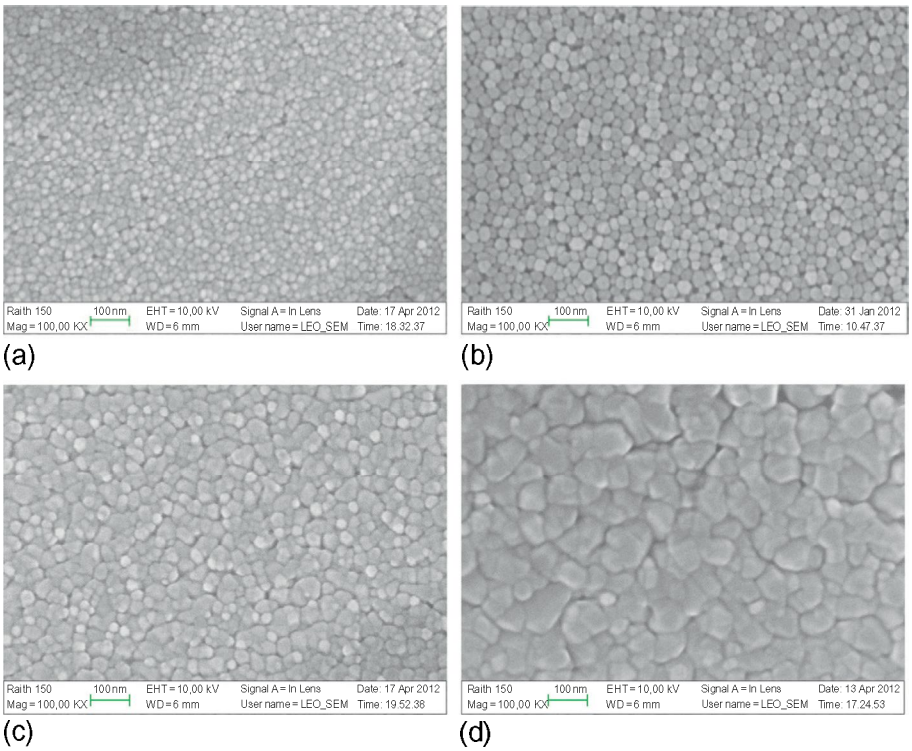

f0020 **Figure 13.3** SEM surface morphology of 3C-SiC (111) grown on Si (111) at $T_C = 550$ °C and different T_S temperatures. (a) 700 °C, (b) 800 °C, (c) 900 °C, (d) 1000 °C.

laser power to induce Si sublimation, making the graphene structure susceptible to more defects and damage. Figure 13.3 shows the surface morphology evolution with increasing substrate temperature. It can be seen that 3C-SiC (111) grown at $T_S = 800$°C is the most uniform among the different growth conditions.

Comp. by: pdjeapradaban Stage: Proof Chapter No.: 13 Title Name: Tewary_and_Zhang
Date:5/12/14 Time:18:14:56 Page Number: 333

B978-1-78242-228-0.00013-2, 00013

s0020 13.3 Laser-induced conversion from 3C-SiC thin film to graphene

p0030 The basic principle of this approach is that a tightly focused laser beam of sufficiently high power density can induce local heating, which may sublimate Si atoms of SiC and leave behind C atoms to recrystallize into graphene layers. Therefore, the general idea is similar to the approach of annealing SiC in high vacuum and high temperature (typically 1200-1600°C) (Shivaraman et al., 2009) to obtain graphene film. This annealing technique has been shown to yield high-quality graphene (e.g., with high electron mobility), in particular on the Si face of SiC where monolayer graphene can be obtained (de Heer et al., 2011). In contrast, our procedure has been carried out under ambient conditions (at room temperature in air), although it can also be performed in vacuum or appropriate gas environment and even under an elevated temperature. A 532 nm continuous wave (CW) Nd-YAG laser with maximum incident power of ~30 mW was used to illuminate and then decompose 3C-SiC (111) grown on Si (111) by MBE into graphene layers. The 532 nm CW laser is an integrated part of a confocal μ-Raman system (LabRAM HR800, Horiba Jobin Yvon). The beam size of 1-2 mm can be focused down to a diffraction limit spot with the size of ~0.7 μm on the sample surface when a 100× objective lens with NA = 0.9 is used. The structural change can be monitored in-situ using μ-Raman. The Raman signal is collected in backscattering geometry. The Raman mapping is carried out by moving the translational stage where the sample sits, controlled with programmable software. With the addition of an external shutter synchronized with the motion control of the translation stage, the illumination site and shape can be controlled to generate different patterns, for instance, dots, lines, or areas. The Raman signal can be obtained simultaneously while the material is being illuminated or probed afterward using lower power. Micron-scale patterns can be obtained by directly using the focused laser beam with a diffraction limit spot size. Even smaller feature sizes (e.g., 100 nm) are possible, if illumination masks are used to define the illumination area or 3C-SiC thin film is selectively deposited in desired patterns. The external and internal shutters are used to control illumination and signal acquisition times, respectively. The laser illumination setup is shown in Figure 13.4, and the phase transformation mechanism is illustrated schematically in Figure 13.5. In the setup described above, the conversion typically requires a laser power of 20-30 mW, depending on the grain structure of the SiC thin film (to be discussed later in detail). In the afterward Raman characterization, the laser power was reduced to 1-2 mW to avoid the laser-heating effect. The Raman spectra of 3C-SiC thin film before and after laser illumination were displayed in Figure 13.6a. It can be clearly seen that three strong peaks of 1348, 1583, and 2691 cm^{-1}, which correspond to D, G, and G' (2D) bands of graphene, emerge after laser illumination. However, the spectrum of the as-grown 3C-SiC on Si (111) does not show these three peaks. A complementary observation is that the intensity of transverse optical phonon mode (TO) of 3C-SiC thin film drops significantly after laser illumination, which implies that the thickness of 3C-SiC decreases due to decomposition or phase change. Because fullerene (C_{60}) was used as a carbon source to grow

Comp. by: pdjeapradaban Stage: Proof Chapter No.: 13 Title Name: Tewary_and_Zhang
Date:5/12/14 Time:18:15:01 Page Number: 334

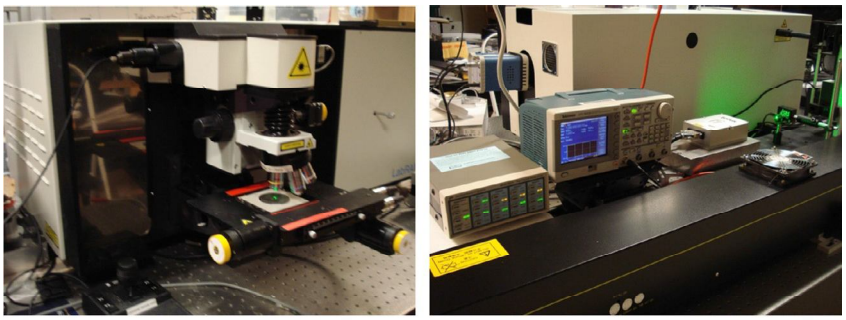

f0025 **Figure 13.4** Laser illumination setup for SiC-to-graphene conversion, (a) showing that a laser beam is focused by a microscope objective lens on an SiC thin-film grown on an Si wafer, and (b) showing a CW 532-nm laser with a mechanical shutter for controlling the illumination time.

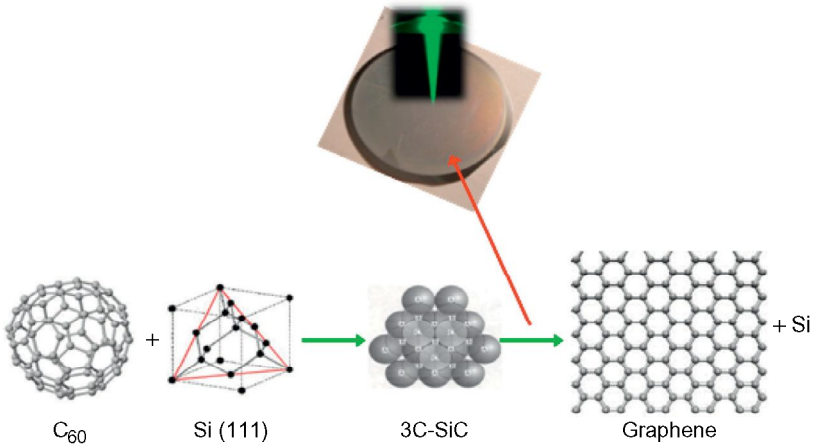

f0030 **Figure 13.5** Schematic illustration of phase transformation of laser-induced SiC to graphene conversion.

3C-SiC on Si (111) and the Raman spectrum of C_{60} was also found to show the D and G bands, there was a possibility that D and G peaks could be from C_{60} after laser illumination. However, the comparison of spectra of laser-illuminated 3C-SiC and C_{60}, as shown in Figure 13.6b, indicates that C_{60} possess only two broad bands D and G, and the double resonant 2D mode only appears in the spectrum of laser-illuminated 3C-SiC. Therefore, the 2D Raman mode is a more reliable confirmation of the graphene layers, and the Raman spectrum confirms the formation of graphene layers on the laser-illuminated 3C-SiC on Si (111).

p0035 In addition to Raman spectroscopy, TEM (JEOL2100) and AFM (Nanoscope SPM V5r30, Veeco) were also used to further confirm the graphene sheets. The *d*-spacing between graphene layers was measured to be about 3.70 Å from TEM image shown in Figure 13.7. The measured spacing is larger than the interlayer spacing of the crystalline graphite with A-B or Bernal stacking ($c/2 = 3.35$ Å), but close to the theoretically predicted graphene layers separation of 3.61 Å (0 K) for the A-A stacking (turbostratic

Comp. by: pdjeapradaban Stage: Proof Chapter No.: 13 Title Name: Tewary_and_Zhang
Date:5/12/14 Time:18:15:01 Page Number: 335

B978-1-78242-228-0.00013-2, 00013

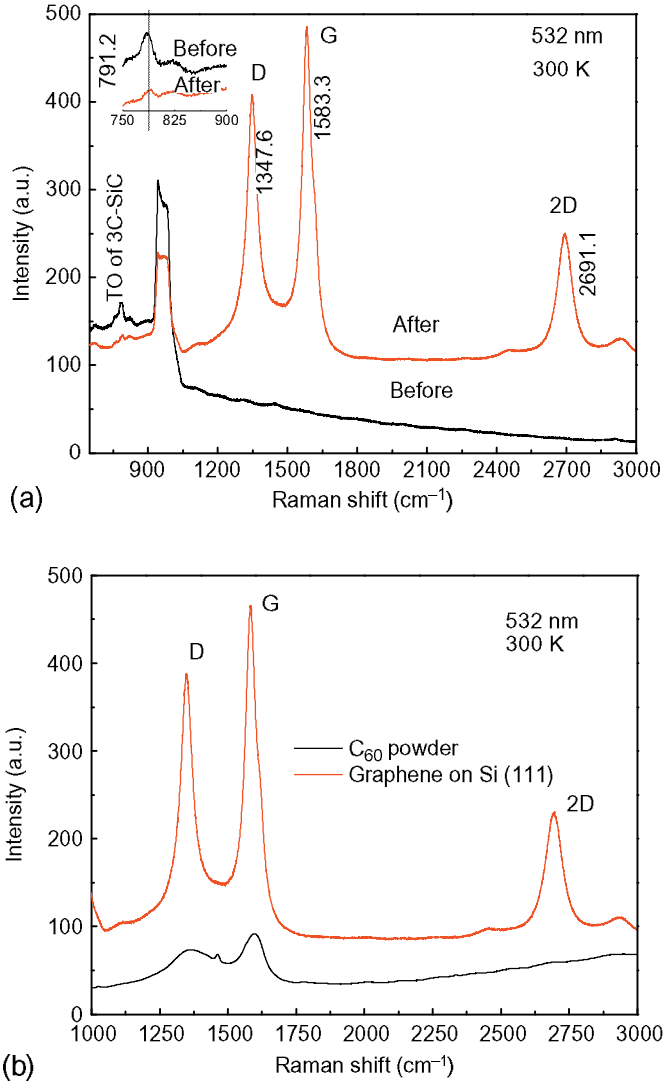

f0035 **Figure 13.6** The Raman spectra of 3C-SiC on Si (111) before and after laser illumination and of C60. (a) 3C-SiC before and after laser illumination, (b) graphene versus C60.

stacking) (Zhang and Tsu, 2010), implying that the stacking order of the multilayer graphene is different from that in the crystalline graphite such as HOPG (Ferrari, 2007) and expected to have weaker interlayer coupling. The turbostratic stacking might result from the fast heating and cooling rates of the laser, which may not give graphene layers enough time to equilibrate into the energetically more favorable stacking order. The number of graphene layers was found to be about eight to nine layers, falling in the range of few-layer-graphene (FLG). As corroborating evidence,

Comp. by: pdjeapradaban Stage: Proof Chapter No.: 13 Title Name: Tewary_and_Zhang
Date:5/12/14 Time:18:15:02 Page Number: 336

B978-1-78242-228-0.00013-2, 00013

f0040

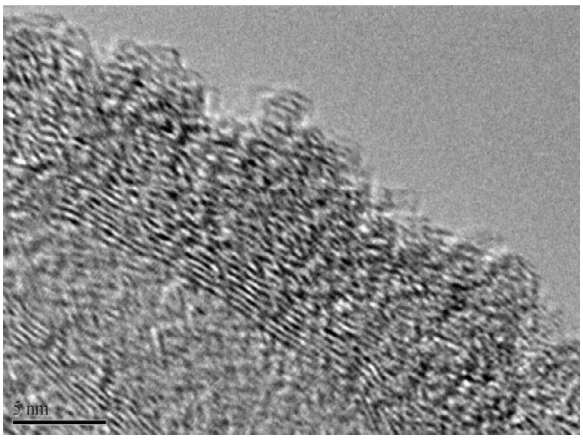

Figure 13.7 TEM micrograph of graphene layers on laser-illuminated 3C-SiC on Si (111).

f0045

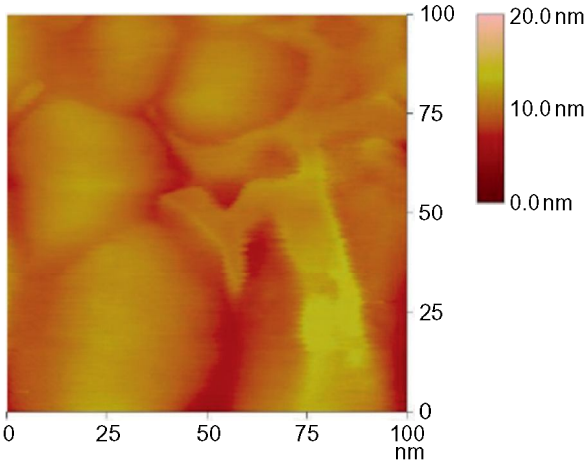

Figure 13.8 AFM topography image of graphene sheet on laser-induced 3C-SiC on Si (111).

the tapping mode AFM image shown in Figure 13.8 reveals a flake with thickness of 3.517 nm, which is approximately the thickness of 3.517/3.7=9-10 layers in agreement with the result from the TEM image.

p0040 To test the feasibility of patterning graphene structures on the SiC film with a laser, we did a 20 μm long line scan under the illumination of ~20 mW of the 532 nm laser. The illuminated line appears darker than the rest area, as revealed in the optical image in Figure 13.9a. The corresponding Raman mapping at the graphene 2D peak was performed with results shown in Figure 13.9b and c. The optical image shown in Figure 13.9a indicates that the line width of about 2 μm results from the laser spot size of about 0.7 μm. The comparison of Raman image shown in Figure 13.9b with optical image shown in Figure 13.9a indicates that the graphene signal distributes uniformly within the ribbon. The comparison between the two Raman spectra from illuminated and nonilluminated areas, as shown in Figure 13.9c, offers an unambiguous confirmation of the SiC-to-graphene conversion. These promising results

Comp. by: pdjeapradaban Stage: Proof Chapter No.: 13 Title Name: Tewary_and_Zhang
Date:5/12/14 Time:18:15:02 Page Number: 337

B978-1-78242-228-0.00013-2, 00013

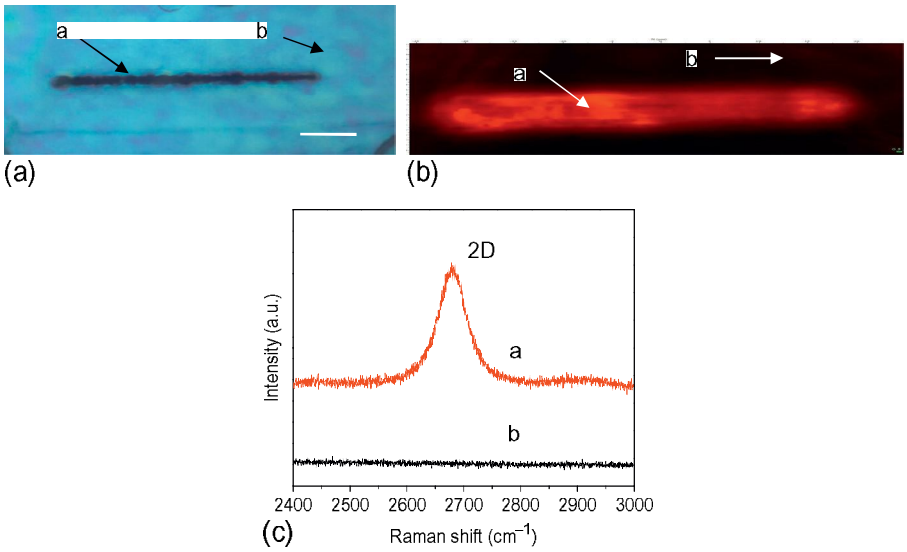

f0050 **Figure 13.9** Raman mapping results of laser-illuminated 3C-SiC on Si (111). (a) Optical image (scale bar: 5 μm), (b) Raman mapping image (image size: $50 \times 10\ \mu m^2$; spectral range: 2650–2750 cm^{-1}), (c) Raman spectra selected from different points.

provide inspiring possibility for patterning electronic devices and electron-photon superstructures.

s0025 13.4 Patterning of periodic graphene micro- or nanostructure for photonic application

p0045 In principle, three approaches can be applied to patterning graphene micro- or nanostructures based on the laser illumination technique: (a) direct writing (DW), (b) prepatterning (PP), and (c) illumination mask (IM), as schematically illustrated in Figure 13.10. Here we concentrate on evaluation of the first two methods. For the direct writing method, as shown in Figure 13.10a, the smallest feature size of the graphene microstructure depends on the laser spot size, which depends on the numerical aperture

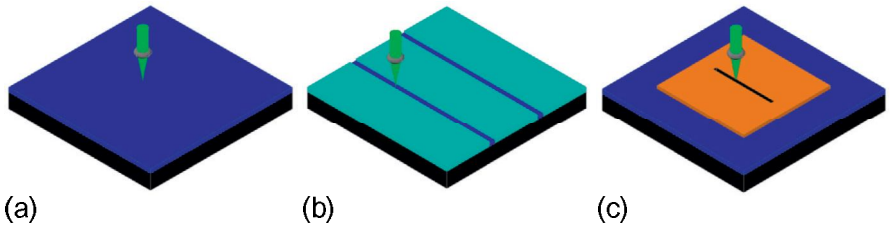

f0055 **Figure 13.10** Three approaches to pattern graphene micro- or nanostructures using laser annealing technique. (a) Direct writing, (b) prepatterning, (c) illumination mask (black-Si, blue-SiC, light blue-SiO_2, brown-illumination mask, and green-laser).

Comp. by: pdjeapradaban Stage: Proof Chapter No.: 13 Title Name: Tewary_and_Zhang
Date:5/12/14 Time:18:15:03 Page Number: 338

B978-1-78242-228-0.00013-2, 00013

(NA) of microscope lens, laser wavelength, laser power, and microstructure of 3C-SiC thin film. Figure 13.11 shows graphene microdiscs formed on three different (111) 3C-SiC on Si (111) samples. The three samples have different surface morphologies and crystalline quality, which requires different threshold laser power values to convert 3C-

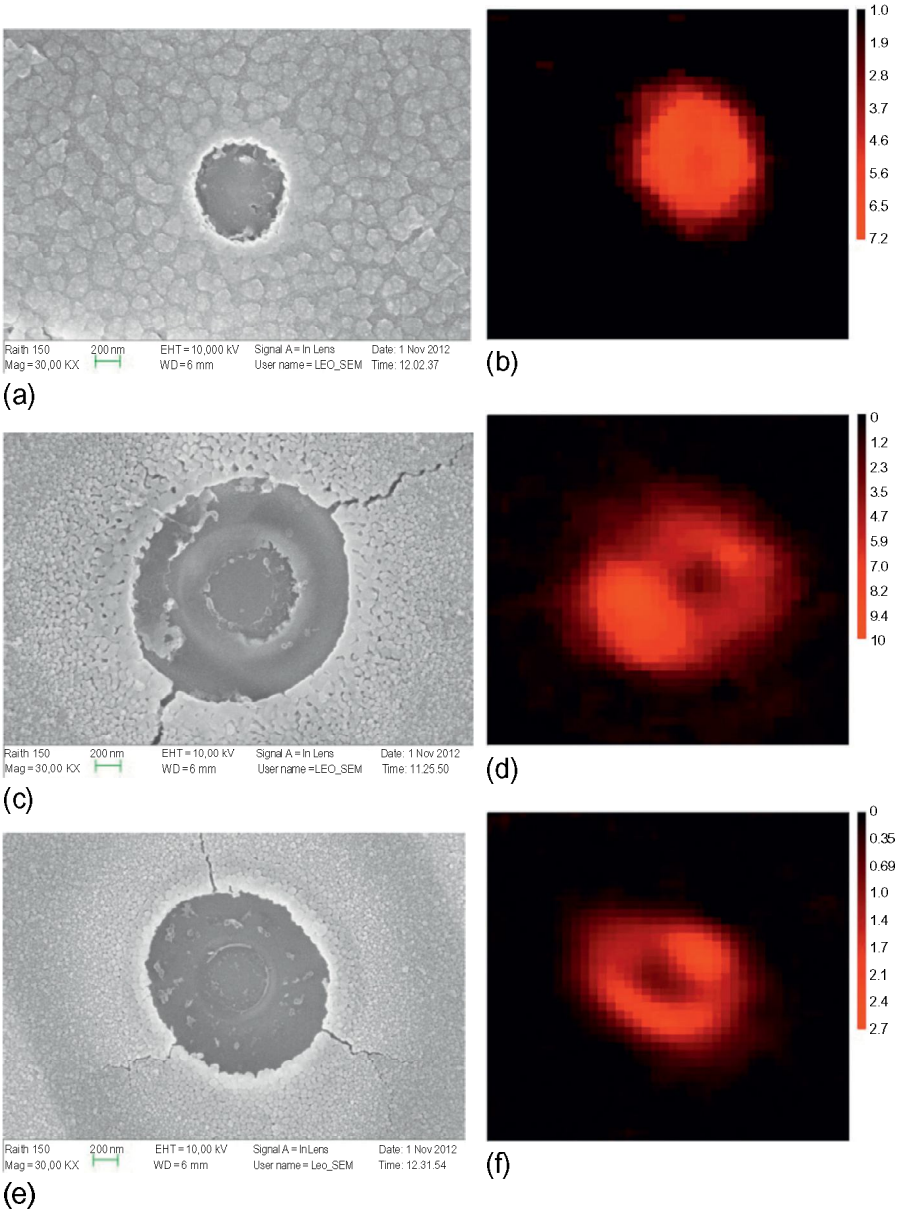

f0060 **Figure 13.11** SEM and corresponding Raman images ($4 \times 4\ \mu m^2$) of three graphene dots illuminated with laser on three samples A, B, and C. (a) and (b) Sample A, (c) and (d) sample B, (e) and (f) sample C (Raman spectral range: 2650–2750 cm^{-1} of graphene 2D peak).

Comp. by: pdjeapradaban Stage: Proof Chapter No.: 13 Title Name: Tewary_and_Zhang
Date:5/12/14 Time:18:15:04 Page Number: 339

B978-1-78242-228-0.00013-2, 00013

SiC into graphene layers. Sample A has a rough surface or highly defective film due to a native SiO_2 layer remaining on the Si substrate, and thus requires the least laser power to induce graphene. Sample B is as thick as sample A, but with fewer defects; therefore, it requires a higher laser power. Sample C is also defective but thinner than sample B; therefore, it requires more laser power than sample B because light absorption is less due to the thinner SiC. Figure 13.11a-f shows SEM micrographs of the laser-induced graphene microdiscs and the corresponding Raman images.

p0050 Similar to the laser patterning process used for generating individual graphene microdiscs, two, four, and nine graphene dots in arrays of 1×2, 2×2, and 3×3 as well as a 10 μm long graphene ribbon were also patterned by programmed laser illumination. Following the patterning of graphene dots, Raman mapping was performed on the patterned areas, with the Raman images shown in Figure 13.12a-d. In comparison with the direct writing method, the prepatterning method via selectively depositing 3C-SiC can enable smaller graphene feature sizes without the limitation of the laser spot size. This approach is based on the finding that C_{60} only reacts with exposed Si but not SiO_2 (Yue et al., 2013). The achievable feature size depends on the

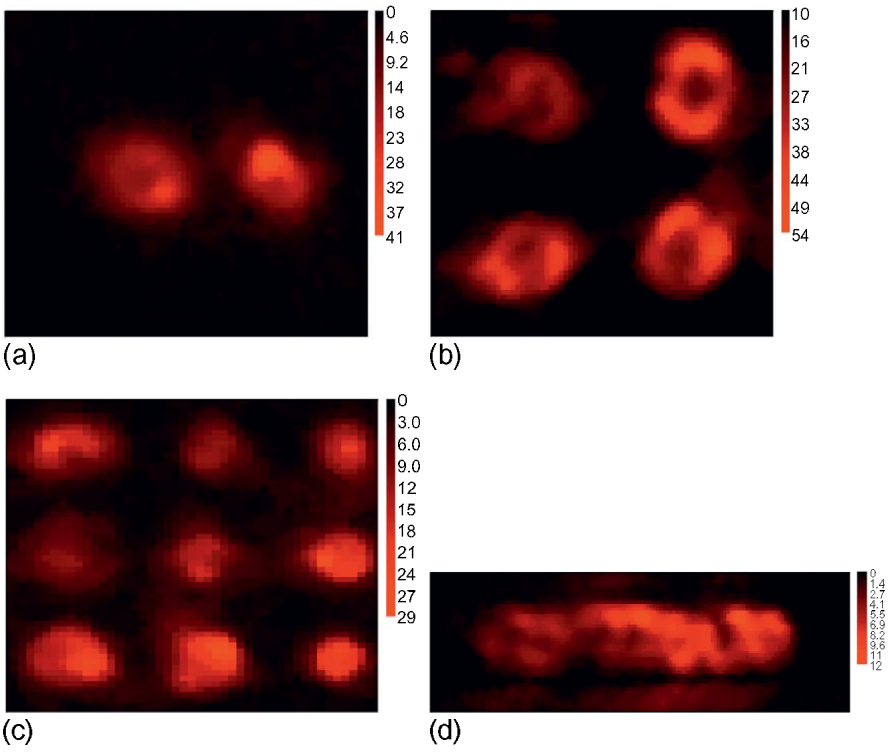

f0065 **Figure 13.12** Raman mapping images (2650–2750 cm^{-1}) of different graphene microdisc arrays and a μ-ribbon. (a) Two dots in (1×2) array (image size: $6\times6\ \mu m^2$), (b) four dots in (2×2) array (image size: $6\times6\ \mu m^2$), (c) nine dots in (3×3) array (image size: $9\times9\ \mu m^2$), (d) a μ-ribbon (image size: $14\times4\ \mu m^2$).

Comp. by: pdjeapradaban Stage: Proof Chapter No.: 13 Title Name: Tewary_and_Zhang
Date:5/12/14 Time:18:15:07 Page Number: 340

B978-1-78242-228-0.00013-2, 00013

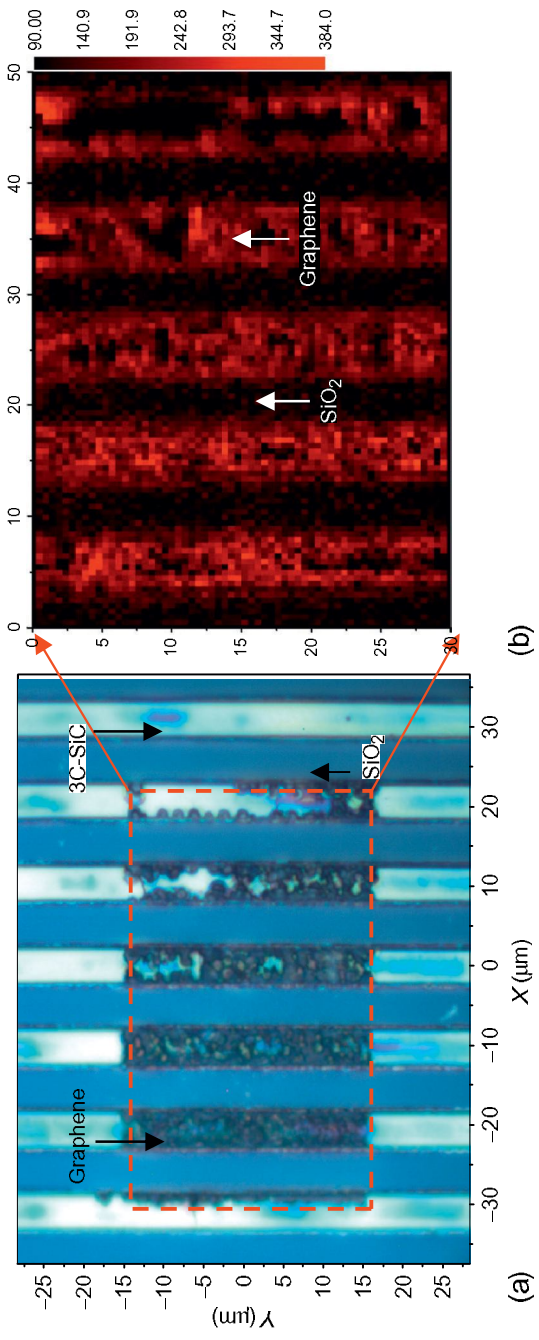

f0070 **Figure 13.13** Optical and Raman images of selective deposited 3C-SiC/Si (111) (5 μm SiC/5 μm SiO_2). (a) Optical image, (b) Raman map image (2650–2750 cm^{-1}).

Comp. by: pdjeapradaban Stage: Proof Chapter No.: 13 Title Name: Tewary_and_Zhang
Date:5/12/14 Time:18:15:10 Page Number: 341

B978-1-78242-228-0.00013-2, 00013

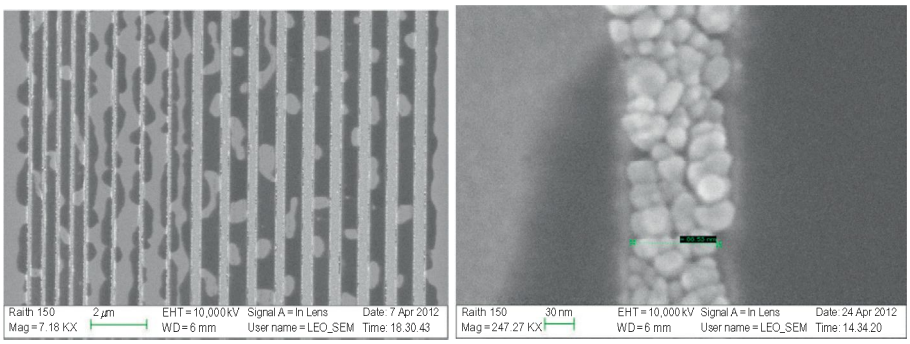

f0075 **Figure 13.14** SEM micrograph of SiC nanowires grown on an Si substrate. (a) Overview, and (b) zoomed-in view for one thin nanowire with ~89 nm width.

capability of photo- or e-beam lithography, dry etching, and selective deposition. We used a photolithographic method to pattern a Si (111) substrate capped with ~100 nm thick SiO_2 and demonstrated the feasibility of this prepattern approach. Figure 13.13a shows an optical image of a laser-illuminated area with selectively deposited 3C-SiC over 5 μm wide silicon strips separated by 5 μm SiO_2 spacers. Figure 13.13b shows the corresponding Raman image of the laser-induced graphene bands. SiC ribbons in nanoscale were also selectively deposited on Si wafers successfully intended to be induced into graphene nanoribbons. The minimum width of SiC nanowire achieved is about 89 nm as shown in Figure 13.14. However, the conversion from SiC nanowire to graphene in the nanoscale presents a new challenge, namely a higher laser power is required, because the heat generated within the ~700 nm focused laser spot is dissipated mostly by the Si wafer, instead of being absorbed by the SiC nanostructure. Therefore, the optimal illumination conditions should be evaluated and identified in the future.

s0030 13.5 Conclusions

p0055 Conventionally, the fabrication of graphene-based devices involves a series of steps including deposition, transfer, and photolithography, which is typically a top-down process. The combination of the selective growth of 3C-SiC on an Si wafer and laser illumination can selectively pattern graphene micro- and nanostructures with required shapes and sizes at any desired location directly on a Si wafer for making graphene-based photonic and electronic devices. This laser-illumination technique may potentially open a route to integrate graphene with existing silicon-based devices. The advantages of laser techniques over other conventional approaches are speed, lower cost, and more flexibility. With the formation of a periodic array, laser-induced graphene can be applied to electronic-photonic superstructure devices. Electron beam lithography can enable the selective deposition of 3C-SiC on Si wafers in nanometer scale and thus produce GNSs for device fabrication.

B978-1-78242-228-0.00013-2, 00013

ac0010 Acknowledgment

The authors acknowledge supports of Army Research Office (ARO), Charlotte Research Institute, and Bissell Distinguished Professorship from UNCC.

References

De Heer, W.A., Berger, C., Ruan, M., Sprinkle, M., Li, X., Hu, Y., Zhang, B., Hankinson, J., Conrad, E., 2011. Large area and structured epitaxial graphene produced by confinement controlled sublimation of silicon carbide. Proc. Natl. Acad. Sci. U. S. A. 108, 16900–16905.

Ferrari, A.C., 2007. Raman spectroscopy of graphene and graphite: disorder, electron-phonon coupling, doping and nonadiabatic effects. Solid State Commun. 143, 47–57.

Hass, J., de Heer, W.A., Conrad, E.H., 2008. The growth and morphology of epitaxial multilayer. J. Phys. Condens. Matter 20, 323202.

Jiao, L., Zhang, L., Wang, X., Diankov, G., Dai, H., 2009. Narrow graphene nanoribbons from carbon nanotubes. Science 458, 877–880.

Kim, K.S., Zhao, Y., Jang, H., Lee, S.Y., Kim, J.M., Ahn, J.H., Kim, P., Ahn, J.H., Kim, P., Choi, J.Y., Hong, B.H., 2009. Large-scale pattern growth of graphene films for stretchable transparent electrodes. Nature (London) 457, 706.

Kosynkin, D.V., Higginbotham, A.L., Sinitskii, A., Lomeda, J.R., Dimiev, A., Price, B.K., Tour, J.M., 2009. Longitudinal unzipping of carbon nanotubes to form graphene nanoribbons. Nature 458 (16), 872–876.

Lee, S., Toney, M.F., Ko, W., Randel, J.C., Jung, H.J., Munakata, K., Lu, J., Geballe, T.H., Beasley, M.R., Sinclair, R., Manoharan, H.C., Salleo, A., 2010. Laser-synthesized epitaxial graphene. ACS Nano 4, 7524–7530.

Li, Y.S., Cai, W.W., An, J.H., Kim, S.Y., Nah, J.H., Yang, D.G., Piner, R., Velamakanni, A., Jung, I. H., Tutuc, E., Banerjee, S.K., Colombo, L., Ruoff, R.S., 2009. Large-area synthesis pf high-quality and uniform graphene films on copper foils. Science 324, 1312–1314, k.

Novoselov, K.S., Geim, A.K., Morozov, S.V., Jiang, D., Zhang, Y., Dubonos, S.V., Grigorieva, I.V., Firsov, A.A., 2004. Electric field effect in atomically thin carbon films. Science 306, 666.

Novoselov, K.S., Geim, A.K., Morozov, S.V., Jiang, D., Katsnelson, M.I., Grigorieva, I.V., Dubonos, S.V., Firsov, A.A., 2005. Two-dimensional gas of massless Dirac fermions in graphene. Nature (London) 438, 197.

Ohkawara, Y., Shinada, T., Fukada, Y., Ohshio, S., Saitoh, H., Hiraga, H., 2003. Synthesis of graphite using laser decomposition of SiC. J. Mater. Sci. 30, 2447–2453.

Perrone, D., Maccioni, G., Chiolerio, A., Martinez de Marigorta, C., Naretto, M., Pandolfi, P., Martino, P., Ricciardi, C., Chiodoni, A., Celasco, E., Scaltrito, L., Ferrero, S., 2009. Study on the possibility of graphene growth on 4H-silicon carbide surfaces via laser processing. In: Proceedings of the Fifth International WLT-Conference on Laser Manufacturing, Munich, June 2009.

Shivaraman, S., Barton, R.A., Yu, X., Alden, J., Herman, L., Chandrashekhar, M.V.S., Park, J., McEuen, P.L., Parpia, J.M., Craighead, H.F., Spencer, M.G., 2009. Free-standing epitaxial graphene. Nano Lett. 9 (9), 3100–3105.

Yannopoulos, S.N., Siokou, A., Nasikas, N.K., Dracopoulos, V., Ravani, F., Papatheodorou, G. N., 2012. CO_2-laser-induced growth of epitaxial graphene on 6H-SiC (0001). Adv. Funct. Mater. 22, 113–120.

Comp. by: pdjeapradaban Stage: Proof Chapter No.: 13 Title Name: Tewary_and_Zhang
Date:5/12/14 Time:18:15:15 Page Number: 343

B978-1-78242-228-0.00013-2, 00013

Yue, N., Zhang, Y., Tsu, R., 2012. Selective formation of graphene on a Si wafer. Mater. Res. Soc. Symp. Proc. 1407. Au1

Yue, N., Zhang, Y., Tsu, R., 2013. Ambient condition laser writing of graphene structures on polycrystalline SiC thin film deposited on Si wafer. Appl. Phys. Lett. 102, 071912.

Zhang, Y., Tsu, R., 2010. Binding graphene sheets together using silicon: graphene/silicon superlattice. Nanoscale Res. Lett. 5, 805–808.

Zhang, Y.B., Small, J.P., Pontius, W.V., Kim, P., 2005. Fabrication and electric-field-dependent transport. Appl. Phys. Lett. 86, 073104.

Comp. by: pdjeapradaban Stage: Proof Chapter No.: 13 Title Name: Tewary_and_Zhang
Date:5/12/14 Time:18:15:15 Page Number: 344